Technical and economic working domains of industrial heat pumps: Part 2 - ammonia-water hybrid absorption-compression heat pumps

Jensen, Jonas Kjær; Ommen, Torben Schmidt; Markussen, Wiebke Brix; Reinholdt, Lars; Elmegaard, Brian

Published in:
International Journal of Refrigeration

Link to article, DOI:
10.1016/j.ijrefrig.2015.02.011

Publication date:
2015

Technical and economic working domains of industrial heat pumps: Part 2 - ammonia-water hybrid absorption-compression heat pumps

Jonas K. Jensen[a,*], Torben Ommen[a], Wiebke B. Markussen[a], Lars Reinholdt[b], Brian Elmegaard[a]

[a]*Technical University of Denmark, Department of Mechanical Engineering, Nils Koppels Alle, Building 403, DK - 2800, Kgs. Lyngby, Denmark*
[b]*Danish Technological Institute, Kongsvang Allé 29 Aarhus, DK-8000, Denmark*

Abstract

The ammonia-water hybrid absorption-compression heat pump (HACHP) has been proposed as a relevant technology for industrial heat supply, especially for high sink temperatures and high temperature glides in the sink and source. This is due to the reduced vapour pressure and the non-isothermal phase change of the zeotropic mixture, ammonia-water. To evaluate to which extent these advantages can be translated into feasible heat pump solutions, the working domain of the HACHP is investigated based on technical and economic constraints. The HACHP working domain is compared to that of the best available vapour compression heat pump with natural working fluids. This shows that the HACHP increases the temperature lifts and heat supply temperatures that are feasible to produce with a heat pump. The HACHP is shown to be capable of delivering heat supply temperatures as high as 150 °C and temperature lifts up to 60 K, all with economical benefits for the investor.

Keywords: Industrial heat pumps, working domain, absorption-compression heat pump, economic evaluation, natural refrigerants

1. Introduction

Industrial scale heat pumps may be applied to improve the energy efficiency of industrial processes (Townsend, D.) or for utility production in urban areas with district heating networks (Ommen et al., 2014). The temperature range where heat pumps for such purposes are applicable is bound by several technical constraints. The technical constraints are governed by the thermodynamic behaviour of the working fluid and the limits of commercially available components, such as compressor discharge temperature and pressure. Further, for a heat pump to be a viable investment, the installation should be the more profitable alternative compared to a competitive technology such as a natural gas burner.

Many industrial scale heat pumps have been installed with a heat supply temperature in range 50-90 °C. The lack of installations above 90 °C is most likely due to the lack of cost efficient solutions in this temperature range, as seen in part 1 of this study (Ommen et al., 2014), rather than a limited demand for high temperature heat pump solutions (Annex 21 , 1995).

The hybrid absorption-compression heat pump (HACHP) or vapour compression heat pump with solution circuit is based on the Osenbrück cycle (Osenbrück, 1895). The advantage of the HACHP is the reduction of vapour pressure and the temperature glides of the absorption and desorption processes, (Altenkirch, 1950; Berntsson and Hultén, 1999, 2002).

The reduction of vapour pressure allows the design of high temperature heat pumps with standard pressure refrigeration components, (Brunin et al., 1997; Jensen et al., 2014). While the non-isothermal phase change allows the temperature profiles of the absorber and desorber to match those of the external circuits, thereby attaining a reduction of the entropy generation caused by heat transfer over a finite temperature difference. Consequently, the HACHP is one feasible measure of approaching the Lorenz cycle (Lorenz, 1894), thereby increasing the efficiency compared to a vapour compression heat pump (VCHP). These advantages make the HACHP a relevant technology, for industrial processes that require high temperatures and large temperature glides.

The HACHP has recently experienced gained interest, as commercial solutions have entered the market. The HACHP has been implemented for waste heat recovery and heat supply in industrial facilities such as dairies, abattoirs, district heating and sewage treatment plants (Hybrid Energy AS, 2015). These installations have a heat load ranging from 150 kW to 1200 kW and a heat supply temperature up to 85 °C (Hybrid Energy AS, 2015).

Brunin et al. (1997) evaluates the working domain of the HACHP based on one technical constraint: maximum pressure and two physical parameters applied as economic indicators: minimum coefficient of performance (COP) and minimum volumetric heat capacity (ratio between heat output and compressor displacement volume). The working domain by Brunin et al. (1997) is evaluated at a fixed 10 K temperature difference, between inlet and outlet, for both the heat sink and heat source. Under these constraints, Brunin et al. (1997) shows that

*Corresponding author

Email addresses: jkjje@mek.dtu.dk (Jonas K. Jensen), tsom@mek.dtu.dk (Torben Ommen), wb@mek.dtu.dk (Wiebke B. Markussen), lre@teknologisk.dk (Lars Reinholdt), be@mek.dtu.dk (Brian Elmegaard)

[1]The original paper was presented on the 11th IIR Gustav Lorentzen Conference on Natural Refrigerants (GL2014), Aug.31 to Sept.2, 2014, Hangzhou, China

Nomenclature

Abbreviations

CRF Capital recovery factor
HACHP Hybrid absorption-compression heat pump
HEX Heat exchanger
LVS Liquid-vapour separator
MRP Manufacturer suggested retail price
NDA Non-disclosure agreement
LP R717 Low pressure R717 components
HP R717 High pressure R717 components
TBP Trade business price
VCHP Vapour compression heat pump

Symbols

A_{HT} Heat transfer area (m^2)
A_{IN} Investment area (m^2)
c Specific energy cost (€ kW^{-1})
c_p Specific heat capacity (kJ kg^{-1} K^{-1})
b Plate press depth (mm)
Bo Boiling number (-)
COP Coefficient of performance (-)
D_h Hydraulic diameter (m)
f Circulation ratio (-)
F Two-phase enhancement factor (-)
FC Annual cost of fuel consumption (€)
h Specific enthalpy (kJ kg^{-1})
h_{fg} Specific heat of vaporization (kJ kg^{-1})
G Mass flux (kg s^{-1} m^{-2})
H Yearly operating time (s)
i Interest rate (-)
i^{eff} Effective interest rate (-)
i_L Inflation rate (-)
L Plate length (m)
LT Technical lifetime (years)
m Mass (kg)
$\dot{m}$ Mass flow rate (kg s^{-1})
M Number of channels (-)
N Number of plates (-)
Nu Nusselt number (-)
NPV Net present value (€)
OMC Operation and maintenance cost (€)
PBP Payback period (years)
PEC Purchased equipment cost (€)
TCI Total capital investment (€)
p Pressure (bar)
Δp Pressure loss (bar)
Pr Prandtl number (-)
PV Present value (€)
q Vapour mass fraction (-)
$\dot{Q}$ Heat rate (kW)
r Relative difference (%)
Re Reynolds number (-)
s Specific entropy (kJ kg^{-1} K^{-1})
T Temperature (°C)
ΔT Temperature difference (K)
t Plate wall thickness (-)
X Size or capacity of component
x Ammonia mass fraction (-)
X_{tt} Lockhart–Martinelli parameter (-)
Z Silver, Bell & Ghaly correlation factor
W Plate width (m)
$\dot{W}$ Power (kW)
U Overall heat transfer coefficient (kW m^{-2} K^{-1})
u_{SL} Superficial liquid velocity (m s^{-1})
u_{SV} Superficial vapour velocity (m s^{-1})
V Volume (m^3)
v Specific volume (m^3 kg^{-1})
$\dot{V}$ Volume flow rate (m^3 s^{-1})

Greek letters

α Heat transfer coefficient (kW m^{-2} K^{-1})
β Plate corrugation angle (°)
γ Cost function exponent (-)
ε Effectiveness (-)
η Efficiency (-)
λ Thermal conductivity (-)
Λ Plate corrugation spacing (m)
μ Viscosity (Pa s)
ϕ Plate area enhancement factor (-)
φ Plate corrugation inclination angle (°)
ξ Pressure drop coefficient (-)

Subscripts

$^-$ Average
c Critical
el Electrical
dis Displacement
HP Heat pump (HACHP)
i Index
is Isentropic
j Stream
k Component
l Liquid
lf Liquid film
lo Liquid only
LM Logarithmic mean
max Maximum
NG Natural gas
pp Pinch point
r Rich
suc Suction line
tp Two phase
v Vapour
vo Vapour only
vol Volumetric
w Wall
W Equipment with known cost
Y equipment with calculated cost

the HACHP can attain allowable heat supply temperatures up to 140 °C with a maximum pressure of 20 bar.

In recent years the maximum pressure for standard refrigeration components have reached 28 bar and further high pressure components have entered the market for R717, allowing a maximum pressure of up to 50 bar, at the time of writing. It is thus relevant to investigate whether the increase in attainable pressures allows higher heat supply temperatures to be reached.

Further, Brunin et al. (1997) does not include the compressor discharge temperature as a constraint but, as discussed in Jensen et al. (2014) the compressor discharge temperature is a limiting factor for the development of a high temperature HACHP.

The use of COP and volumetric heat capacity as indicators for the economic viability of a heat pump investment may not always lead to a precise conclusion, as discussed in part 1 of this study (Ommen et al., 2014). This is because components for different refrigerants may vary in cost due to e.g. different material requirements or different heat transfer coefficients and thus, the level of COP needed to attain a viable investment will differ based on the level of investment required for the specific refrigerant. Evaluating the working domain based on a complete economic evaluation of the heat pump installation, over the lifetime of the system may result in valuable information not provided by Brunin et al. (1997).

Further, the application of a complete economic analysis allows the different heat pump solutions to be compared based on an objective measure. Thus, evaluating the difference in the expected economic gain of the investment and thereby identifying the most relevant technologies.

Ommen et al. (2011) compared the economy of the HACHP to the VCHP and showed that the HACHP is a competitive technology. However, the study did not consider the degradation of heat transfer coefficients caused by the application of a zeotropic mixture working fluid. As discussed in Radermacher and Hwang (2005) the two-phase heat transfer coefficient is reduced due to mass diffusion resistance in the zone surrounding the liquid-vapour interface, which tends to be depleted of the volatile component. Consequently, the HACHP requires a larger heat transfer area compared to a pure R717 VCHP. Further, the reduced vapour pressure of the mixture increases the specific volume of the low pressure vapour and consequently entails the need for an increased compressor displacement volume. It is therefore relevant to evaluate, whether this increased investment in heat transfer area and compressor volume can be justified by the increased efficiency of the heat pump.

Due to the use of a mixed working fluid and the solution circuit configuration the design of the HACHP has two additional degrees of freedom. Both Brunin et al. (1997) and Ommen et al. (2011) use a fixed ammonia mass fraction and the concentration difference (difference between ammonia concentration in the rich mixture and the circulated lean mixture) to satisfy these additional degrees of freedom. Jensen et al. (2014) applies the ammonia mass fraction and circulation ratio to determine the operation of the cycle and presents parameter variations of these. This shows that it is essential to determine the right combination of ammonia mass fraction and circulation ratio to attain a feasible high temperature HACHP, that complies with the constraints of commercially available components and further that the right combination is highly dependent on the operating conditions. As both Brunin et al. (1997) and Ommen et al. (2011) have restricted their HACHP analysis to a limited number of ammonia mass fractions and used a fixed value of concentration difference the HACHP is not necessarily analysed under the best possible design conditions, which may result in an unfair comparison.

Ommen et al. (2014) shows that the heat sink and heat source temperature differences have a significant influence on both the economic and technical constraints of VCHPs. Ommen et al. (2014) investigates four cases with different combinations of heat sink and heat source temperature differences. These are:

- ΔT_{sink} =10 K, ΔT_{source} =10 K
- ΔT_{sink} =20 K, ΔT_{source} =20 K
- ΔT_{sink} =20 K, ΔT_{source} =10 K
- ΔT_{sink} =40 K, ΔT_{source} =10 K

The same four cases will be applied in the present study of HACHP. In the following they will be referred to as sink/source configuration: 10K/10K, 20K/20K, 20K/10K and 40K/10K. The definition of ΔT_{sink} and ΔT_{source} is presented in detail in Sec. 2.1 and is presented graphically in Fig. 1b.

This study investigates the working domain of the HACHP for these four cases. For each case the operating conditions, defined by the heat supply temperature, $T_{\text{sink,out}}$, and the temperature lift, ΔT_{lift}, will be varied. The heat supply temperature from 40-140 °C and the temperature lift from 0-70 K. For each operating condition the ammonia mass fraction and circulation ratio are found by an optimisation of the net present value (NPV) under the technical constraints of the studied components. The working domains are presented graphically for all four cases, showing which operating conditions are possible to supply with a HACHP while respecting both the technical and economic constraints. Finally, the present value (PV) of the HACHP will be compared to the PV of the best available VCHP technology presented by Ommen et al. (2014).

2. Methods

2.1. The hybrid absorption-compression heat pump process

The general layout of the HACHP is seen in Fig. 1a. In the desorber, heat is supplied from a heat source, stream 13-14, in order to desorb the ammonia from the mixture. The phase change in the desorber is incomplete and thus stream 1 exiting the desorber is a liquid-vapour mixture. By separating the phases in a liquid-vapour separator (LVS), it can be ensured that only the vapour phase, stream 2, enters the compressor, while the liquid phase, stream 8, is supplied to the pump. The liquid stream will be lean in ammonia while the vapour stream consists mainly of ammonia. After the pump the lean mixture, stream 9, is heated in an internal Heat Exchanger (HEX) resulting in stream 10 which is mixed with stream 3, the vapour exiting the compressor. This causes an adiabatic absorption of the

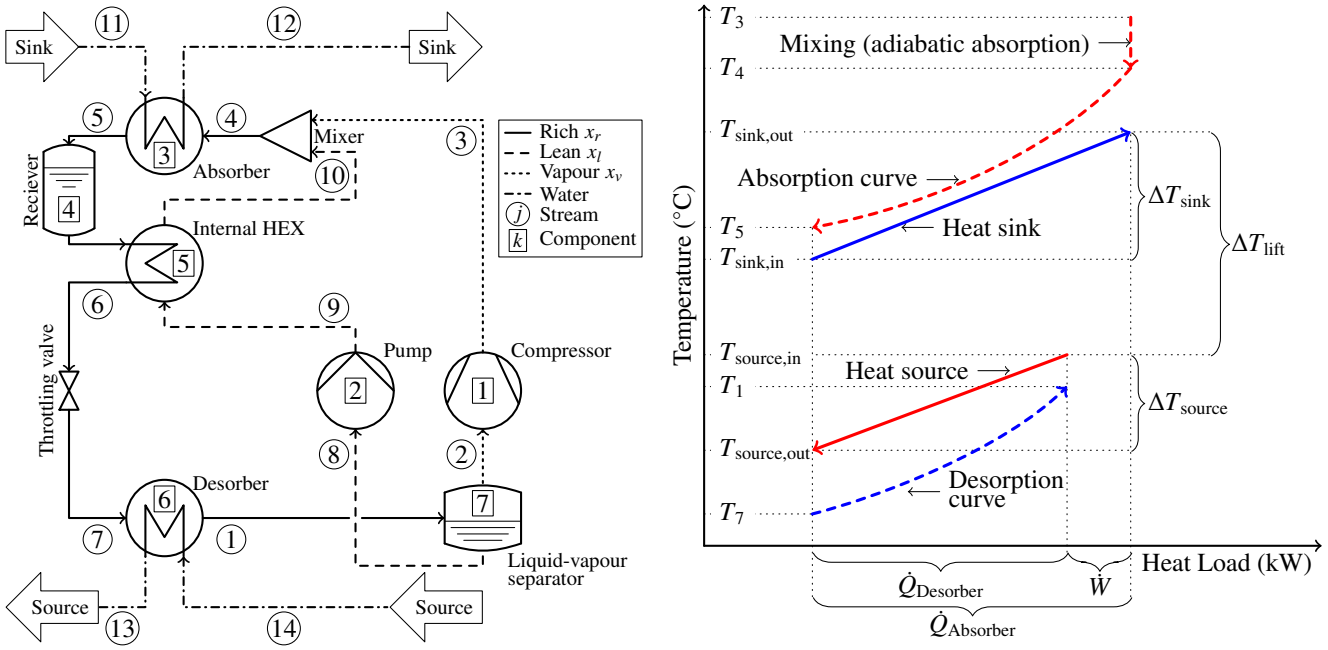

Figure 1: (a) Principle sketch of the HACHP, (b) HACHP process sketched in a temperature - heat load diagram

vapour phase into the lean liquid until equilibrium is reached, resulting in stream 4. In the absorber a diabatic absorption of the ammonia vapour into the liquid is undertaken, while releasing heat to the heat sink, stream 11-12. The exiting state, stream 5, is a saturated liquid mixture. As it is beneficial to sub-cool this stream, it is used as the heat source in the internal HEX. After this the sub-cooled liquid mixture, stream 6, is throttled to the low pressure resulting in a two-phase stream that enters the desorber, stream 7.

The process described above is sketched in a principle temperature – heat load diagram shown in Fig. 1b. Here the applied definitions of temperature lift, ΔT_{lift}, and heat sink and heat source temperature difference, ΔT_{sink} and ΔT_{source}, are illustrated. As seen ΔT_{lift} was defined as the temperature difference between the heat supply temperature, $T_{\text{sink,out}}$, and the temperature of the available heat source, $T_{\text{source,in}}$. ΔT_{sink} and ΔT_{source}, were defined as the temperature difference between the inlet and outlet of the sink and source, respectively.

From Fig. 1b it may be seen that the profiles of the equilibrium absorption and desorption processes are non-linear. This has been described in detail by Itard and Machielsen (1994). In Fig. 1b these are depicted as convex curves. Depending on ammonia mass fraction and circulation ratios these profiles could also exhibit a concave shape or have a convex and a concave part. This is further described in Zheng et al. (2013). When modelling the HACHP it is accordingly not sufficient to only ensure a positive temperature difference at the inlet and outlet of the absorber and desorber (Itard and Machielsen, 1994).

Table 1: Fixed input variables applied in the thermodynamic model of the HACHP

Input variable			Components to which they are applied	
η_{is}	0.80	-	Compressor	Pump
η_{vol}	0.80	-	Compressor	
η_{el}	0.95	-	Compressor	Pump
ΔT_{pp}	5.00	K	Absorber	Desorber
ε	0.90	-	Internal HEX	
$\dot{Q}$	1000	kW	Absorber	

2.2. *Thermodynamic model of the hybrid absorption-compression heat pump*

The thermodynamic model of the HACHP was developed based on mass and energy balance equations and the second law of thermodynamics. Steady-state operation was assumed. Design variables were chosen on a component and system level. Component design variables were: isentropic and volumetric efficiency, η_{is} and η_{vol}, for compressor and pump, heat exchanger effectiveness, ε, for the internal HEX and the minimum temperature difference (in the following, referred to as the *pinch point* temperature difference), ΔT_{pp}, for the absorber and desorber. The applied values are stated in Table 1. On a system level the design variables were chosen as the ammonia mass fraction of the rich solution, x_r, (streams 4-7 and 1) and the circulation ratio, f, defined as the ratio between the mass flow rate of the rich and lean mixture, Eq. (1).

$$f = \frac{\dot{m}_l}{\dot{m}_r} \tag{1}$$

Based on the high pressure, p_5 and low pressure, p_1, all other pressures in the system were determined. Pressure losses

in piping and vessels were neglected. For the high pressure side:

$$p_6 = p_5 - \Delta p_{5-6} \quad (2)$$

$$p_4 = p_5 + \Delta p_{4-5} \quad (3)$$

$$p_3 = p_{10} = p_4 \quad (4)$$

$$p_9 = p_{10} - \Delta p_{9-10} \quad (5)$$

Likewise for the low pressure side:

$$p_7 = p_1 + \Delta p_{7-1} \quad (6)$$

$$p_2 = p_8 = p_1 \quad (7)$$

The values of Δp were determined from the HEX correlations described in detail in Sec. 2.3

Based on the mass balance of the LVS it was found that the circulation ratio, f, directly relates to the vapour quality exiting the desorber, such that $q_1 = 1 - f$. Thereby the thermodynamic state of stream 1 was defined by x_r, q_1 and p_1.

Heat loss from the LVS was neglected and thermodynamic equilibrium between the two phases was assumed, hence: $T_1 = T_8 = T_2$. Stream 2 was assumed to be saturated vapour ($q_2 = 1$). The ammonia mass fraction and enthalpy of the lean liquid (stream 8) were found by energy, mass and element balances of the LVS.

The specific enthalpy of streams 3 and 9 were found using the isentropic efficiencies of the pump and the compressor. Heat loss from these components were neglected.

The heat transfer of the internal HEX was found by the Eq. (8), which was derived from an energy balance of the internal HEX and the definition of the heat exchanger effectiveness.

$$\dot{Q}_5 = \dot{m}_l \left(h_{10,max} - h_9\right) \varepsilon_5 \quad (8)$$

Here $h_{10,max}$ is the enthalpy of the lean solution evaluated at the temperature of stream 5, as the capacity rate of the rich solution is higher than the lean solution.

The enthalpy of stream 4 was calculated based on the energy and mass balances of the mixer. The throttling valve was assumed to be isenthalpic, $h_6 = h_7$.

The heat transfer rates and power consumption of the components were calculated by component energy balances, Eqs. (9) to (13).

$$(1)\quad \text{Compressor:} \qquad \dot{W}_1 = \dot{m}_v \left(h_3 - h_2\right) \quad (9)$$

$$(2)\quad \text{Pump:} \qquad \dot{W}_2 = \dot{m}_l \left(h_9 - h_8\right) \quad (10)$$

$$(3)\quad \text{Absorber:} \qquad \dot{Q}_3 = \dot{m}_r \left(h_4 - h_5\right) \quad (11)$$

$$(5)\quad \text{Internal HEX:} \qquad \dot{Q}_5 = \dot{m}_r \left(h_5 - h_6\right) \quad (12)$$

$$(6)\quad \text{Desorber:} \qquad \dot{Q}_6 = \dot{m}_r \left(h_1 - h_7\right) \quad (13)$$

The COP of the HACHP was defined as given in Eq. (14). The electrical efficiency of the electric motors driving the pump and compressor, η_{el}, was assumed to be the same for both the pump and compressor. The applied value of η_{el} is stated in Table 1.

$$\text{COP} = \frac{\dot{Q}_3}{\dot{W}_1 + \dot{W}_2} \cdot \eta_{\text{el}} \quad (14)$$

Table 2: Plate dimensions for V120 T and V10 T, variable designation on the plate is seen in Fig. 2

	V120 T	V10 T	
L	456	243	(-)
L_{HT}	525	289	(-)
W	243	119	(mm)
β	30	30	(°)
Λ	8.0	8.0	(mm)
b	1.8	1.8	(mm)
t	0.5	0.5	(mm)
λ	16.0	16.0	($\text{Wm}^{-1}\text{K}^{-1}$)

Table 3: Applied heat transfer and pressure drop correlations for the absorber, desorber and internal heat exchanger

Absorber				
Water	α:	Martin (1996)	ξ:	Martin (1996)
NH_3-H_2O	α_{vo}:	Martin (1996)		
	α_{lf}:	Yan et al. (1999)		
	α_{tp}:	Silver (1947), Bell and Ghaly (1972)	ξ_{tp}:	Yan et al. (1999)
Internal HEX				
NH_3-H_2O	α:	Martin (1996)	ξ:	Martin (1996)
Desorber				
Water	α:	Martin (1996)	ξ:	Martin (1996)
NH_3-H_2O	α_{lo}:	Martin (1996)	ξ_{lo}:	Martin (1996)
	α_{tp}:	Táboas et al. (2012)	ξ_{tp}:	Táboas et al. (2012)

The displacement volume of the compressor, $\dot{V}_{\text{dis}}$, was found by Eq. (15), here $\dot{V}_{\text{suc}}$ is the suction line volume flow rate, calculated as seen in Eq. (16), and η_{vol} is the volumetric efficiency of the compressor.

$$\dot{V}_{\text{dis}} = \frac{\dot{V}_{\text{suc}}}{\eta_{\text{vol}}} \quad (15)$$

$$\dot{V}_{\text{suc}} = \dot{m}_2 \cdot v_2 \quad (16)$$

The thermodynamic model was implemented in the software Engineering Equation Solver (F-Chart, 1992). The thermodynamic properties of the ammonia-water mixture were calculated by the equations of state developed by Ibrahim and Klein (1993). Transport properties were calculated using correlations developed by El-Sayed (1985) and Conde (2004)

The model was implemented such that all equations are explicit for defined high and low pressure, p_5 and p_1. These pressures were solved iteratively to attain the desired values of the absorber and desorber ΔT_{pp}.

As enthalpy and temperature are not proportional during absorption and desorption, the absorber and desorber models were discretized equidistantly in heat load. From this the temperature difference for each step, ΔT_i, was evaluated based on the equilibrium temperature of the ammonia-water mixture. The pinch point temperature difference was then determined as seen in Eq. (17).

$$\Delta T_{\text{pp}} = \min(\Delta T_i) \quad i \in \{1; I\} \quad (17)$$

I=50 steps was applied to both the absorber and desorber to determine the pinch point temperature differences.

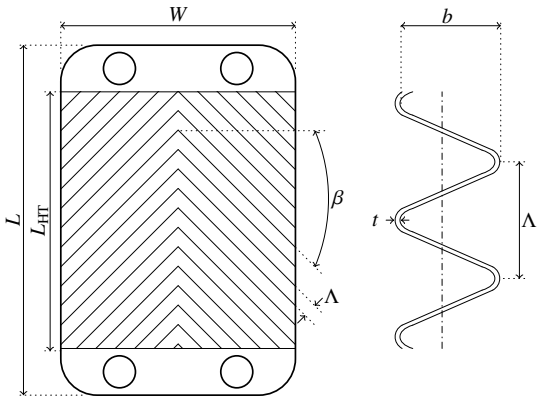

Figure 2: Plate dimension for chevron corrugation

2.3. Dimensioning heat exchangers

All three heat exchangers were assumed to be of a plate type with a chevron corrugation, as depicted in Fig. 2. The use of plate heat exchangers for industrial processes have increased significantly over the last decades (Abu-Khader, 2012) and is therefore assumed to be the preferred option.

The plate size correspond to either the "V120T" or the "V10T" (SWEP international AB, 2014), for which a complete list of the applied dimensions are given in Table 2. The small plate size (V10T) was applied when the pressure loss using the large plate (V120T) exceeds Δp=0.5 bar. This tends to happen when there is a large difference in the mass flow rate between the exchanging fluids. This occurred in the absorber and desorber when ΔT_{sink} and ΔT_{source} were small and in the internal HEX when the circulation ratio, f, was large.

As the plate size was given, the objective of the HEX dimensioning was to determine the number of plates, N, needed to attain a heat transfer area, A_{HT}, capable of transferring the required heat load, $\dot{Q}$. These parameters relate as seen in Eq. (18).

$$A_{\text{HT}} = N \cdot L_{\text{HT}} \cdot W \cdot \phi = \frac{U \cdot \Delta T_{\text{LM}}}{\dot{Q}} \tag{18}$$

Here U is the overall heat transfer coefficient of the HEX and ΔT_{LM} is the logarithmic mean temperature difference. Further, L_{HT} is the length of the heat transfer section of the plate, W is the plate width and ϕ is the plate area enhancement factor calculated as suggested by Martin (1996) (see Appendix A) to account for the complex geometry of the channels. The area for which the cost has been correlated, A_{IN}, is the full area of the purchased plates and is thus determined as seen in, Eq. (19).

$$A_{\text{IN}} = N \cdot L \cdot W \cdot \phi \tag{19}$$

The overall heat transfer coefficient was calculated as the inverse of the sum of the convective resistance of both streams and the conductive resistance through the plate, see Eq. (20).

$$U = \left(\frac{1}{\bar{\alpha}_1} + \frac{t}{\lambda} + \frac{1}{\bar{\alpha}_2} \right)^{-1} \tag{20}$$

Here, $\bar{\alpha}$ is the average heat transfer coefficient of the individual streams, t is the plate thickness and λ is the thermal conductivity of the plate. Detailed heat transfer coefficient correlations were applied to both the absorber, desorber and internal HEX to determine $\bar{\alpha}$. The applied correlations are listed in Table 3 and the equations are stated in Appendix A.

The HEX pressure losses, Δp, were calculated as seen in Eq. (21).

$$\Delta p = \frac{2 \cdot \bar{\xi} \cdot G^2 \cdot v \cdot L_{\text{HT}}}{D_h} \tag{21}$$

Here G is the mass flux and D_h is the hydraulic channel diameter, set to $D_h = 2b\phi$ as suggested by Martin (1996). Further, $\bar{\xi}$ is the average friction factor, which was determined based on the correlations listed in Table 3 the equations are equally presented in Appendix A.

For the sink and source streams of the absorber and desorber and both streams in the internal HEX $\bar{\alpha}$ and $\bar{\xi}$ were evaluated at the mean temperature and pressure. This is a reasonable approach as the transport properties of the liquids only show a weak dependence on the pressure and temperature.

For the ammonia-water streams of the absorber and desorber this approach was not applicable as the ammonia mass fraction of the liquid and vapour phase changes through the HEX, which can lead to significant variations in the transport properties of the two phases. Further, α and ξ are strongly dependent on the vapour quality, q which also varies greatly during absorption and desorption. To account for these variations $\bar{\alpha}$ and $\bar{\xi}$ were determined based on a one-dimensional discretization in heat load and averaged as seen in Eqs. (22) and (23).

$$\bar{\alpha}_{\text{tp}} = \left(\sum_{i=1}^{I} \alpha_{\text{tp},i} \right) \cdot I^{-1} \tag{22}$$

$$\bar{\xi}_{\text{tp}} = \left(\sum_{i=1}^{I} \xi_{\text{tp},i} \right) \cdot I^{-1} \tag{23}$$

Here $\alpha_{\text{tp},i}$ and $\xi_{\text{tp},i}$ are the two-phase heat transfer coefficient and friction factor for the i^{th} cell, calculated based on the cell averages of: vapour quality, temperature, pressure and liquid and vapour ammonia mass fraction.

Further, for the absorber and desorber the logarithmic mean temperature difference could not be directly applied as enthalpy and temperature are not proportional during absorption and desorption (Itard and Machielsen, 1994; Zheng et al., 2013). To account for this an average logarithmic mean temperature difference was defined as seen in Eq (24).

$$\Delta \bar{T}_{\text{LM}} = \left(\sum_{i=1}^{I} \Delta T_{\text{LM},i} \right) \cdot I^{-1} \tag{24}$$

Here $\Delta T_{\text{LM},i}$ is the logarithmic mean temperature difference of the i^{th} cell calculated by the same discretization as applied in the heat transfer correlation ($I = 50$).

2.4. Refrigerant charge estimation and dimensioning of high pressure receiver

Based on the calculated size of the three heat exchangers the working fluid charge, m, was estimated by evaluating the

Table 4: Fixed parameters applied in the economic analysis

Interest rate	i	7 %
Inflation rate	i_L	2 %
Technical lifetime	LT	15 years
Operating time	H	3500 hours pr. year
Gas burner efficiency	η_{NG}	0.9 -
Gas burner investment cost	TCI_{NG}	0 €
Gas burner maintenance cost	OMC_{NG}	0 €

volume occupied by the working fluid and the mean specific volume, $\bar{v}$, of the HEX, see Eq. (25)

$$m_k = M_k \cdot W_k \cdot b_k \cdot \frac{1}{\bar{v}_k} \tag{25}$$

Here M is the number op channels occupied by the working fluid. The total m_{tot} was defined as the sum of the working fluid charge in the absorber, desorber and internal HEX.

The high pressure receiver was dimensioned such that it can contain the entire charge at the high pressure (state of stream 5). The receiver was over-sized by 25% as suggested by Stoecker (1998). The receiver volume, V_4, was calculated as stated in Eq. (26).

$$V_4 = (m_3 + m_5 + m_6) \cdot v_5 \cdot 1.25 \tag{26}$$

The application of an oversized high pressure receiver ensures a saturated state at the outlet from the absorber (stream 5, Fig. 1a) (Corberan, 2011).

2.5. Compressors and technological constraints

The maximum heat supply temperature achievable by a heat pump is restricted by the maximum pressure of the applied compressor technology. Further, the maximum achievable temperature lift is restricted by the compressor discharge temperature and in some cases differential pressure. This is to ensure the thermal stability of the lubricating oil and to reduce wear by thermal stress. As discussed in Ommen et al. (2014), the compressor discharge temperature is of special concern for ammonia heat pumps.

In the present study two compressor technologies were investigated: low pressure ammonia (Ommen et al. (2014): Type 3) and high pressure ammonia (Ommen et al. (2014): Type 4). The low pressure ammonia compressor (LP R717) has a maximum pressure of 28 bar. The discharge temperature is limited to 180 °C. The high pressure ammonia compressor (HP R717) has a maximum pressure of 50 bar and can equally tolerate discharge temperatures up to 180 °C.

Generally the water content in the compressed vapour stream is negligible but as shown by Jensen et al. (2014): for low ammonia mass fractions the water content can be substantial for some operating conditions. These solutions should be avoided and therefore solutions with $x_v < 0.95$ were deemed infeasible.

2.6. Economic evaluation

The basis of the economic analysis was the replacement of an existing gas burner with a HACHP of the same heat load. Thus, it was necessary to evaluate the total capital investment

Table 5: Used cost correlations coefficients for the component types divided by application limits

Equipment	PEC_W	X_W	γ	Source
Compressor:	(€)	($\text{m}^3\ \text{h}^{-1}$)		
LP R717	11914	178.4	0.66	TBP [1,2]
HP R717	NDA	NDA	NDA	MRP [4]
Electrical motor:	(€)	(kW)		
LP/HP R717	10710	250.0	0.65	TBP[1]
Receiver:	(€)	(m^3)		
LP R717	1444	0.089	0.63	TBP[1]
HP R717	1934	0.089	0.66	TBP[1]
Plate HEX:	(€)	(m^2)		
LP R717	15526	42.0	0.80	TBP[1,2,3]
HP R717	NDA	NDA	NDA	MRP[5]
Pump:	(€)	(kW)		
LP/HP R717	NDA	NDA	NDA	MRP[6]
LVS:	(€)	($\text{m}^3\ \text{h}^{-1}$)		
LP/HP R717	12702	525	0.39	TBP[1]

[1]H. Jessen Jürgensen A/S (2013), [2]FK Teknik A/S (2013)
[3]Ahlsell Danmark ApS (2013), [4]Johnson Controls (2013)
[5]SWEP International AB (2015), [6]Grundfos DK A/S (2014)

(TCI) of the HACHP. To determine TCI_{HP}, first the purchased equipment cost (PEC) of all major components was found. PEC functions were developed for all major components based on Danish intermediate trade business prices (TRB) and individual manufacturers suggested retail prices (MRP). The cost functions were constructed as proposed by Bejan et al. (1996), see Eq. (27).

$$\text{PEC}_Y = \text{PEC}_W \left(\frac{X_Y}{X_W} \right)^{\gamma} \tag{27}$$

Here PEC_Y is the PEC of the component at capacity X_Y, while PEC_W is the PEC at a chosen base capacity, X_W. The correlated capacities for the different components were as follows:

- PEC for a compressor was a function of the compressor displacement volume and the pressure limit.
- PEC for an electrical motor with a fixed efficiency was dependent only on the shaft power.
- PEC for a heat exchanger was a function of the HEX area and the pressure limit.
- PEC for a pump was a function of the shaft power.
- PEC for a LVS was a function of the compressor suction line volume flow rate. The size was chosen to attain a vapour velocity of 0.4 m/s in the separator. This corresponds to an entrained liquid droplet size with a maximum diameter of 0.25 mm (Stoecker, 1998).
- PEC for a high pressure receiver was a function of the volume and pressure limit.

The values of PEC_W, X_W and γ attained are stated in Table 5 together with the source from which the cost information was supplied. Cost information for some components were supplied under a non-disclosure agreement (NDA) and thus the coefficients of the developed cost functions are not published.

Once the PEC costs of all components were determined the total capital investment (TCI) of the HACHP installation was found. As suggested by Bejan et al. (1996), it was assumed that the TCI was a factor of 4.16 higher than the PEC of the component, Eq. (28).

$$\mathrm{TCI_{HP}} = \sum_{k=1}^{K} \mathrm{PEC}_k \cdot 4.16 \tag{28}$$

The factor of 4.16 was applied to account for additional costs related to new investment at an existing facility. It was thus applied to account for additional direct costs such as: piping, instrumentation and control, electrical equipment, civil and structural work and service facilities as well as indirect costs such as: engineering and supervision costs and construction and contractor profit costs (Bejan et al., 1996).

Annual costs for the fuel consumption of both the existing gas burner and the proposed HACHP was determined as seen in Eqs. (29) and (30) (Bejan et al., 1996), respectively.

$$\mathrm{FC_{NG}} = \frac{\dot{Q}}{\eta_{\mathrm{NG}}} \cdot c_{\mathrm{NG}} \cdot H \tag{29}$$

$$\mathrm{FC_{HP}} = \frac{\dot{Q}}{\mathrm{COP}} \cdot c_w \cdot H \tag{30}$$

Here c_{NG} and c_w are the natural gas and electricity prices, H is the operating time per year and η_{NG} is the assumed gas burner efficiency. The applied values of H and η_{NG} are stated in Table 4, while c_{NG} and c_w corresponding to an industrial consumer in the Danish fiscal environment for year the 2012, prices from Danish Energy Agency (2013) were applied.

To account for the time value of money the capital recovery factor (CRF), see Eq. (31) (Bejan et al., 1996), was applied to discount future expenditure to a PV.

$$\mathrm{CRF} = \frac{i^{\mathrm{eff}}(1+i^{\mathrm{eff}})^{\mathrm{LT}}}{(1+i^{\mathrm{eff}})^{\mathrm{LT}}-1} \tag{31}$$

As seen in Eq. (31), CRF depends on the effective interest rate over the life time of the system, i^{eff}, and the technical life time LT. The effective interest rate was calculated from the interest rate, i, and inflation rate, i_L, as seen in Eq. (32) (Bejan et al., 1996). The assumed value of LT ,i and i_L are stated in Table 4.

$$i^{\mathrm{eff}} = \frac{1+i}{1+i_L} - 1 \tag{32}$$

The PV of the two alternatives: keeping the natural gas burner or replacing it with a HACHP was found using Eq. (33).

$$\mathrm{PV}_i = \mathrm{TCI}_i + \frac{\mathrm{FC}_i}{\mathrm{CRF}} + \mathrm{OMC}_i \tag{33}$$

For the natural gas burner the capital investment was assumed as sunk costs ($\mathrm{TCI_{NG}}$=0 €) and further the operation and maintenance cost (OMC) were neglected ($\mathrm{OMC_{NG}}$=0 €). Thus, $\mathrm{PV_{NG}}$ is equivalent to the discounted FC over the technical life time of the project. For the HACHP the OMC were assumed to attain a PV equivalent to 20% of the TCI as suggested by Bejan et al. (1996).

The criteria for the economic viability of the HACHP installation was a positive NPV when replacing a natural gas boiler as the source of heat supply. The NPV was defined as the difference in PV of the two alternatives as seen in Eq. (34).

$$\mathrm{NPV} = \mathrm{PV_{NG}} - \mathrm{PV_{HP}} \tag{34}$$

Thus, if the NPV is positive the HACHP investment will be profitable while if the NPV is negative keeping the natural gas burner would be the more profitable solution.

Further, a simple pay back period (PBP) was determined as stated in Eq. (35). The PBP is calculated as the ratio of the $\mathrm{TCI_{HP}}$ and the yearly savings in running costs.

$$\mathrm{PBP} = \frac{\mathrm{TCI_{HP}}}{(\mathrm{FC_{NG}} - \mathrm{FC_{HP}}) + (\mathrm{OMC_{NG}} - \mathrm{OMC_{HP}}) \cdot \mathrm{CRF}} \tag{35}$$

PBP is not a precise measure of the economic viability of an investment as it does not account for the time value of money and thus should be used with caution (Bejan et al., 1996). However, PBP is often used as a selection criterion in industry typically with a maximum allowable value (Bejan et al., 1996). The maximum PBP is not easily defined as this depends highly on the industry and the type of investment. For the present study PBPs of 4 and 8 years will be reported, however the overall criteria for the economic viability will be NPV > 0 €, regardless of the actually allowed PBP. NPV = 0 € indicates that the PBP equals the technical lifetime of the system, which was assumed to be 15 years.

3. Results

Detailed results from one run of the thermodynamic, heat transfer and economic model are provided in Appendix B. The results are provided for x_r = 0.65 and f = 0.65, an operating condition of $T_{\mathrm{sink,out}}$ = 80 °C and ΔT_{lift} = 30 K and a sink/source configuration of 20K/20K

3.1. The influence of x_r and f on the HACHP working domain

Fig. 3 shows the HACHP working domain for two fixed combinations of x_r and f. Fig. 3a has a high ammonia mass fraction of x_r = 0.9 while 3b has a low ammonia mass fraction of x_r = 0.5. The circulation ratio, f, was chosen to give high values of COP and thus as suggested by Jensen et al. (2014) the circulation ratio is reduced with an increase in ammonia mass fraction. Fig. 3a has a circulation ratio of f = 0.35 while 3b has a circulation ratio of f = 0.85.

The working domains in Fig. 3 are presented with the heat supply temperature, $T_{\mathrm{sink,out}}$, as the abscissa and the temperature lift, ΔT_{lift}, as the ordinate. Further, a fixed sink/source configuration of 10K/10K is applied and thus ΔT_{sink} and $\Delta T_{\mathrm{source}}$ are both fixed at a value of 10 K. Thus, for a given $T_{\mathrm{sink,out}}$: $T_{\mathrm{sink,in}}$ is determined from ΔT_{sink}. Likewise, from a given ΔT_{lift} and

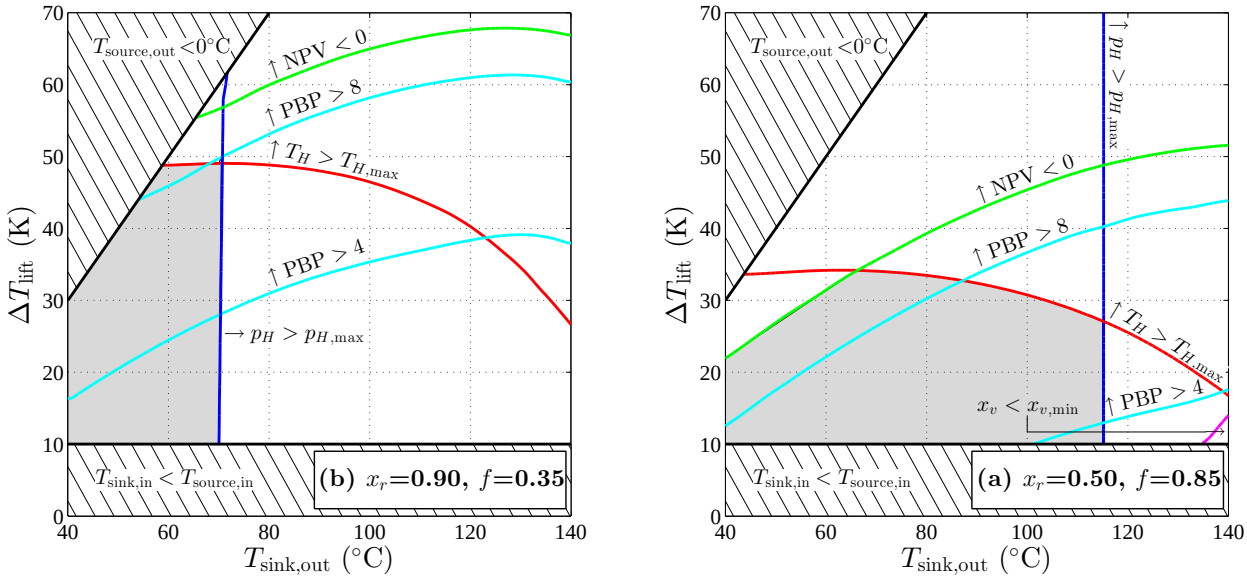

Figure 3: Working domain for a HACHP with fixed ammonia mass fraction and circulation ratio. (a) x_r = 0.90 and f = 0.35, (b) x_r = 0.50 and f = 0.85. Both for a sink/source configuration of 10K/10K. The technical and economic constraints correspond to the LP R717 components

$T_{\text{sink,out}}$: $T_{\text{source,in}}$ is determined and finally $T_{\text{source,out}}$ is found from ΔT_{source}.

The hatched areas in Fig. 3 define operating conditions for which heat pump implementation is not applicable. The upper left corner indicates operating points that are infeasible as these require $T_{\text{source,out}}$ < 0 °C, which implies a phase change for the chosen heat transfer fluid (water). This could be feasible if a brine was applied. However, it should be noted that this also implies cooling the heat source well below ambient temperature, which might not be reasonable unless a cooling demand is met.

The bottom rectangle indicates operating points at which $T_{\text{sink,in}} < T_{\text{source,in}}$. These operating points are neglected as for these conditions, direct heat transfer between the sink and source is possible for some range of the heat transfer process. Therefore, this should be applied first, as suggested by the principles of pinch analysis (Kemp , 2011; Townsend, D.).

The resulting working domains are indicated in Fig. 3 by the gray areas. These areas represent values of $T_{\text{sink,out}}$ and ΔT_{lift} where the HACHP simultaneously complies with all technical and economic constraints.

Further, all constraints are presented in Fig. 3. The dark blue line indicates the $T_{\text{sink,out}}$ and ΔT_{lift} at which the high pressure is equal to the maximum allowable pressure, $p_{H,\max}$, for Figs. 3a and 3b 28 bar, corresponding to LP R717 components. Solutions to the left of the blue line thus have high pressures within the limit of the applied technology, while solutions to the right of the blue line have pressures above the allowable limit and are thus infeasible. As seen, the high pressure constraint only shows a weak dependence on ΔT_{lift}. Further, it is seen that the $T_{\text{sink,out}}$ at which $p_{H,\max}$ is reached differs significantly for the two values of x_r presented. As seen in Fig. 3a with x_r = 0.9: heat supply temperature of only 70 °C can be reached while, as seen in Fig. 3b with x_r = 0.5: a heat supply temperature up to 115 °C can be attained.

The red line indicates the $T_{\text{sink,out}}$ and ΔT_{lift} at which the compressor discharge temperature is equal to the maximum allowable temperature, $T_{H,\max}$. As seen $T_{H,\max}$ depends mainly of ΔT_{lift}. Hence, solutions with $T_{\text{sink,out}}$ and ΔT_{lift} below the red line have compressor discharge temperatures below $T_{H,\max}$ while solutions with $T_{\text{sink,out}}$ and ΔT_{lift} above the red line exceed the limitations of $T_{H,\max}$ and are thus infeasible. As seen the higher the $T_{\text{sink,out}}$ the lower the ΔT_{lift} is possible. When comparing the compressor discharge temperature constraint in Figs. 3a and 3b it is clear that the choice of ammonia mass fraction has an impact on attainable temperature lifts. As seen a reduction of the ammonia mass fraction entails a reduction of the attainable temperature lift.

The green line indicates the $T_{\text{sink,out}}$ and ΔT_{lift} at which the NPV of the investment is zero and thus where the installation of a HACHP is equivalent to keeping the existing natural gas burner. Solutions with $T_{\text{sink,out}}$ and ΔT_{lift} below the green line have positive NPV and are thus economically feasible while solutions above the green line have a negative NPV and are thus not economically viable.

As seen, NPV is dependent on both $T_{\text{sink,out}}$ and ΔT_{lift}, because an increase in ΔT_{lift} decreases the COP and consequently increases the annual fuel costs. Further, increasing ΔT_{lift} for a given $T_{\text{sink,out}}$ reduces the temperature level of the heat source, which results in a reduction of the low pressure and consequently an increased suction line volume flow and the need for a larger compressor investment. Likewise, increasing $T_{\text{sink,out}}$ for a given ΔT_{lift} increases the temperature of the heat source subsequently resulting in a reduced compressor investment.

When comparing the NPV constraint in Figs. 3a and 3b it is clear that the choice of ammonia mass fraction also influences

NPV. As seen a reduction of the ammonia mass fraction reduces the number of economically viable solutions. This is due to the an increase in TCI_{HP} caused by the sum of three phenomena:

- The reduction of vapour pressure results in an increased suction line volume flow rate, and thus a large compressor investment.
- The reduction of the two-phase heat transfer coefficient, results in a larger absorber and desorber investment.
- The increase in circulation ratio increases the heat transfer in the internal HEX and thus the internal HEX investment

The light blue lines indicate the $T_{\text{sink,out}}$ and ΔT_{lift} at which the PBP is 4 and 8 years, respectively. As seen the PBP follows the same trend as the NPV.

Finally, the magenta line, seen only in the bottom right corner of Fig. 3b, indicates the $T_{\text{sink,out}}$ and ΔT_{lift} at which the ammonia mass fraction of the vapour stream supplied to the compressor is equal to the minimum allowable value. Solutions below this line are thus infeasible as these have too low a vapour ammonia mass fraction.

When comparing the two working domains presented in Figs. 3a and 3b it is clear that the choices of ammonia mass fraction and circulation ratio influence the amount of feasible HACHP solutions. As seen, when the ammonia mass fraction is high temperature lifts up to 49 K can be attained, while the HACHP under these conditions is only capable of reaching a heat supply temperature of 70 °C. Conversely, the low ammonia mass fraction solution is capable of reaching heat supply temperatures up to 115 °C but can only attain temperature lifts up to 35 K.

Consequently, defining the HACHP working domain based on fixed values of ammonia mass fraction and circulation ratio may not fairly represent the strengths and limitations of the HACHP technology as a whole.

3.2. Optimization of x_r and f to determine complete HACHP working domain

In order to assess the complete working domain of the HACHP technology, a selection criterion was defined to choose the economically optimal design at each operating condition (defined by $T_{\text{sink,out}}$ and ΔT_{lift}). Values of x_r and f have been set individually for each computed operating condition for all four cases, to maximize the NPV of the installation. The technical constraints of the high pressure, p_H, compressor discharge temperature, T_H, and vapour ammonia mass fraction, x_v, have been imposed on the optimization of NPV.

Figs. 4a and 4b show the optimum value of x_r and f, respectively, for a sink/source configuration of 10K/10K and with the application of the HP R717 components. The corresponding COP is presented in Fig. 4c, and TCI in Fig. 4d. As seen the optimum value of x_r is 0.9 up to a heat supply temperature of approximately, $T_{\text{sink,out}}$ = 100 °C. At this point the high pressure with x_r = 0.9 attains a value 50 bar, corresponding to the limits of the HP R717 compressor. When increasing the supply temperature beyond this point the ammonia mass fraction must consequently be reduced to comply with the high pressure constraint. All optimal solutions beyond this point have the maximum allowable pressure and thus the maximum allowable ammonia mass fraction. This is in alignment with what was shown in Fig. 3 and is also in alignment with the conclusions of studies such as Berntsson and Hultén (1999, 2002).

From Fig. 4b it is be seen that optimal choice of f remains close to constant as long as x_r = 0.9, while it starts to increase when the ammonia mass fraction is reduced.

As seen from Fig. 4c the COP increases slightly up to the point at which the ammonia mass fraction is reduced. Moving beyond this point COP decreases slightly. However, it is seen that the COP is more sensitive to the value of ΔT_{lift} than to $T_{\text{sink,out}}$.

Fig. 4d shows that the TCI decreases up to the point at which the ammonia mass fraction is reduced. The reduction of TCI combined with the increased COP results in an improved NPV up to the point at which $p_{H,\text{max}}$ is reached. Moving beyond this point, TCI increases while COP decreases, thus reducing NPV. However, it may be seen that the increase of the investment flattens out for $T_{\text{sink,out}}$ > 120 °C. This occurs as the higher temperatures increase the specific volume in the suction line thus countering the increase due to the reduction of x_r. Further, going below an x_r of approximately 0.5 will cause the two-phase heat transfer coefficient to increase again as pure water is approached.

3.3. HACHP working domain

Figs. 5 and 6 show the derived working domains of the HACHP under the four investigated sink/source configuration cases and under the application of both the LP R717 and HP R717 components.

Fig. 5 shows the working domain for the sink/source configurations of 10K/10K (5a & 5b) and 20K/20K (5c & 5d). Figs. 5a and 5c correspond to the use of the LP R717 components while the HP R717 components have been applied in Figs. 5b and 5d.

Fig. 6 shows the working domain for the sink/source configuration of 20K/10K (6a & 6b) and 40K/10K (6c & 6d). Equally, Figs. 6a and 6c are for LP R717 components, while Figs. 6b and 6d are with the HP R717 components.

As in Fig. 3 the grey areas in Figs. 5 and 6 indicate the operating conditions that comply with all technical and economic constraints. Further, all constraints are presented as in Fig. 3. However, it should be noted that the dashed blue line presented in Figs. 5 and 6 indicate the point at which the optimal solution attains the maximum allowable pressure. Thus, all solutions to the left of the dashed blue line have pressures below $p_{H,\text{max}}$ while all solutions to the right of the dashed blue line have $p_H = p_{H,\text{max}}$. The solutions to the right of dashed blue line are thus feasible solutions but they operate on the pressure boundary to attain the best economy.

As may be seen from Fig. 5a, the HACHP using the LP R717 components at a sink/source configuration of 10K/10K

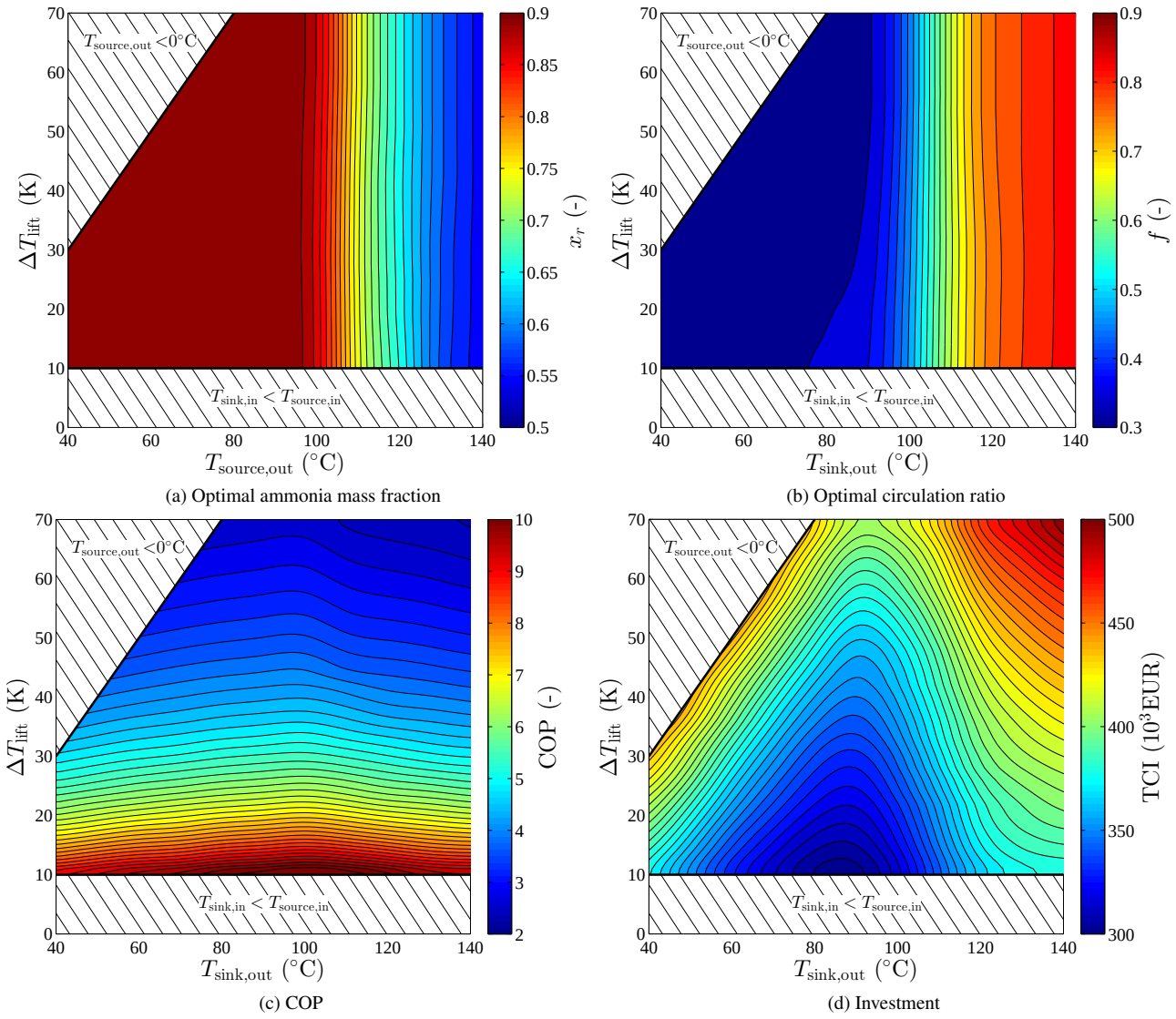

(a) Optimal ammonia mass fraction

(b) Optimal circulation ratio

(c) COP

(d) Investment

Figure 4: Optimal choice of x_r and f and the corresponding COP and TCI for a sink/source configuration of 10K/10K

can deliver a maximum heat supply temperature of $T_{\text{sink,out}}$ = 125 °C and a maximum temperature lift of ΔT_{lift} = 48 K. It can be seen that the maximum heat supply temperature is limited by the vapour ammonia mass fraction, x_v, while the maximum temperature lift is limited by the compressor discharge temperature. Further, it may be seen that all technically feasible solutions attain a positive NPV and almost all attain a simple PBP lower than 8 years. To attain a PBP below 4 years a maximum temperature lift of 28 K can be attained at a heat supply temperature of 65 °C.

Applying the HP R717 compressors to the 10K/10K sink/source configuration, the maximum heat supply temperature is increased to above $T_{\text{sink,out}}$ = 140 °C, see Fig. 5b. Further, it can be seen that the maximum lift of 48 K can be retained at higher heat supply temperatures when applying the high pressure compressor. It can be seen that the maximum heat supply temperature and maximum temperature lift are both bound by the compressor discharge temperature. Again all technically feasible solutions attain a positive NPV.

For the sink/source configuration of 20K/20K, Figs. 5c and 5d, the maximum temperature lift is 42 K while the maximum heat supply temperature is 119 °C for LP R717 and 130 °C for HP R717. For 20K/10K, Figs. 6a and 6b, this is reduced to a maximum temperature lift of 54 K and a maximum heat supply temperature of 125 °C for LP R717 and 135 °C for HP R717. For sink/source configuration 40K/10K, Figs. 6c and 6d, the maximum temperature lift is 60 K while the maximum heat supply temperature is 100 °C and 125 °C for LP and HP R717 respectively.

It can be seen that mainly the working domain for the LP R717 compressor at a sink/source configuration of 10K/10K is bound by the x_v constraint. For 20K/10K a minor area is also limited by x_v. All other working domains are limited entirely by the compressor discharge temperature. Further, all technically feasible solutions have a positive NPV and almost all have a PBP below 8 years. In general, when increasing the sink

glide the maximum heat supply temperature is reduced while the maximum lift is increased.

3.4. Best available HACHP and comparison with the VCHP

From Figs. 5 and 6 it can be seen that the working domains of the LP and HP R717 components overlap in the low temperature range. It is therefore relevant to evaluate when it is more profitable to chose a high pressure solution over the low pressure solution. Fig. 7 shows which component technology yields the highest possible NPV for all four evaluated sink/source configurations. As seen, this results in two regions: a low temperature region (blue) in which the LP R717 components should be used and a high temperature region (yellow) in which the HP R717 components should be used. The supply temperature at which the high pressure option becomes favourable is approximately $T_{\text{sink,out}}$ = 75 °C for 10K/10K, $T_{\text{sink,out}}$ = 85 °C for 20K/20K, $T_{\text{sink,out}}$ = 78 °C for 20K/10K and $T_{\text{sink,out}}$ = 90 °C for 40K/10K. If this is compared to the dashed blue lines in Figs. 5 and 6 it may be seen that the switch from LP to HP R717 happens approximately 5-8 °C above the point where the LP R717 reaches $p_{H,\text{max}}$. This is due the retention of the high ammonia mass fraction for the HP R717 meaning that the compressor volume will be smaller and the heat transfer coefficient will be higher. Hence, the HP R717 investment becomes smaller than the LP R717 investment although the investment in the HP R717 components are higher per unit of displacement volume and heat transfer area.

Further, Fig. 7 shows the working domain of the best available VCHP, as concluded from Ommen et al. (2014). As seen, the HACHP competes mainly with low and high pressure R717 and R600a but also with R744 for 40K/10K. Comparing the working domain of the HACHP to the working domain of the best possible VCHP solution it is clear that the HACHP expands the range of operating conditions for which heat pump application is technically feasible and economically viable. The HACHP allows both higher temperature lifts and higher heat supply temperatures, especially when ΔT_{sink} is large.

Fig. 7 also shows the difference in cost between the HACHP and the VCHP. This is represented by the relative difference in present value: r_{PV}=((PV_{VCHP}-PV_{HACHP})/PV_{VCHP})·100%. As seen, r_{PV} is between -5.0% and +9% for the range in which low pressure HACHP competes with low pressure R717. For low pressure HACHP against high pressure R717, r_{PV} is between -1.0% and +19% while high pressure HACHP versus high pressure R717 results in r_{PV} is between -1.0% and +17%.

For the range where the HACHP competes with R600a the r_{PV} is between 23% and 78%. This is due to the large investment and poor COP associated with R600a. Hence, for heat supply temperatures above $T_{\text{sink,out}}$ = 90 °C where R717 can no longer be applied, the HACHP seem to be the more profitable solution.

Also for the range where LP HACHP competes with the transcritical R744 heat pump, the HACHP seem to be the preferred option with r_{PV} between 9-18%.

Fig. **??** shows the trend of r_{PV} for the sink/source configuration of 10K/10K. As seen, the economic advantage of the HACHP is larger at low temperature lifts. Further, it may be seen that the advantage increases with increasing heat supply temperature. Fig. **??** shows the relative difference in COP between the HACHP and VCHP: r_{COP}=(($\text{COP}_{\text{HACHP}}$ - COP_{VCHP}) / COP_{VCHP})·100%. As seen, the HACHP offers significantly increased COP at low lifts. However, when the temperature lift is increased the COP of the HACHP and the VCHP approach one another. This as the advantage of the HACHP is the reduction of irreversibilities related to the heat exchange processes. However, as the temperature lift is increased the irreversibilities related to the compression is more dominant and thus the efficiency of the two systems become similar. This results in the trend of r_{PV} seen in Fig. **??**. As seen, for low temperature range (LP R717 versus LP HACHP), where compressor investment is high, this results in an area where the HACHP is not economically favourable compared to the VCHP. This is indicated by the red line in Fig. **??**.

As seen from Fig. 7 the HACHP offers the best economic improvement for the sink/source configuration of 20K/10K. One could expect the improvement to be even higher for 40K/10K due to the large sink temperature difference, but this is not the case as a high sink temperature difference also entails a high temperature lift and thus the HACHP and VCHP are only compared at lifts where the COP is similar.

4. Discussion

Comparing R717 VCHP to the HACHP, the r_{PV} for most operating points is between 5-10%. However, the PEC cost of commercial components may vary with up to 40% from the indicated price. This might be an advantage for large manufactures where large quantities are purchased and PEC thereby can be reduced. This could cause the R717 VCHP to attain equal or higher NPV as VCHPs are a more mature technology with more competition between the suppliers. As shown in Ommen et al. (2014) one of the highest uncertainty on the NPV is related to the electricity price. An increased electricity cost would be an advantage for the HACHP over the VCHP due to the higher COP, while a reduction of the electricity price would be an advantage for the VCHP as the NPV would be more influenced by investment.

Further, the performance of VCHP could be further optimized by the application of exergoeconomic optimization (Bejan et al., 1996) to the temperature difference in the evaporator and condenser. This would allow the best trade-off between investment and running cost to be determined for each refrigerant and at each operating point. This, however could also be applied to HACHP. If exergoeconomic optimization was applied the technologies would be compared at the best possible design, which might change the conclusion from this study.

Further, the HACHP is just one method for vapour compression systems to approach the Lorenz cycle. Conventional vapour compression heat pumps set in series are an alternative measure of this. This could prove to be a more cost efficient solution and should be investigated.

It should be noted that the application of the high pressure compressor to the HACHP did not increase the range of feasi-

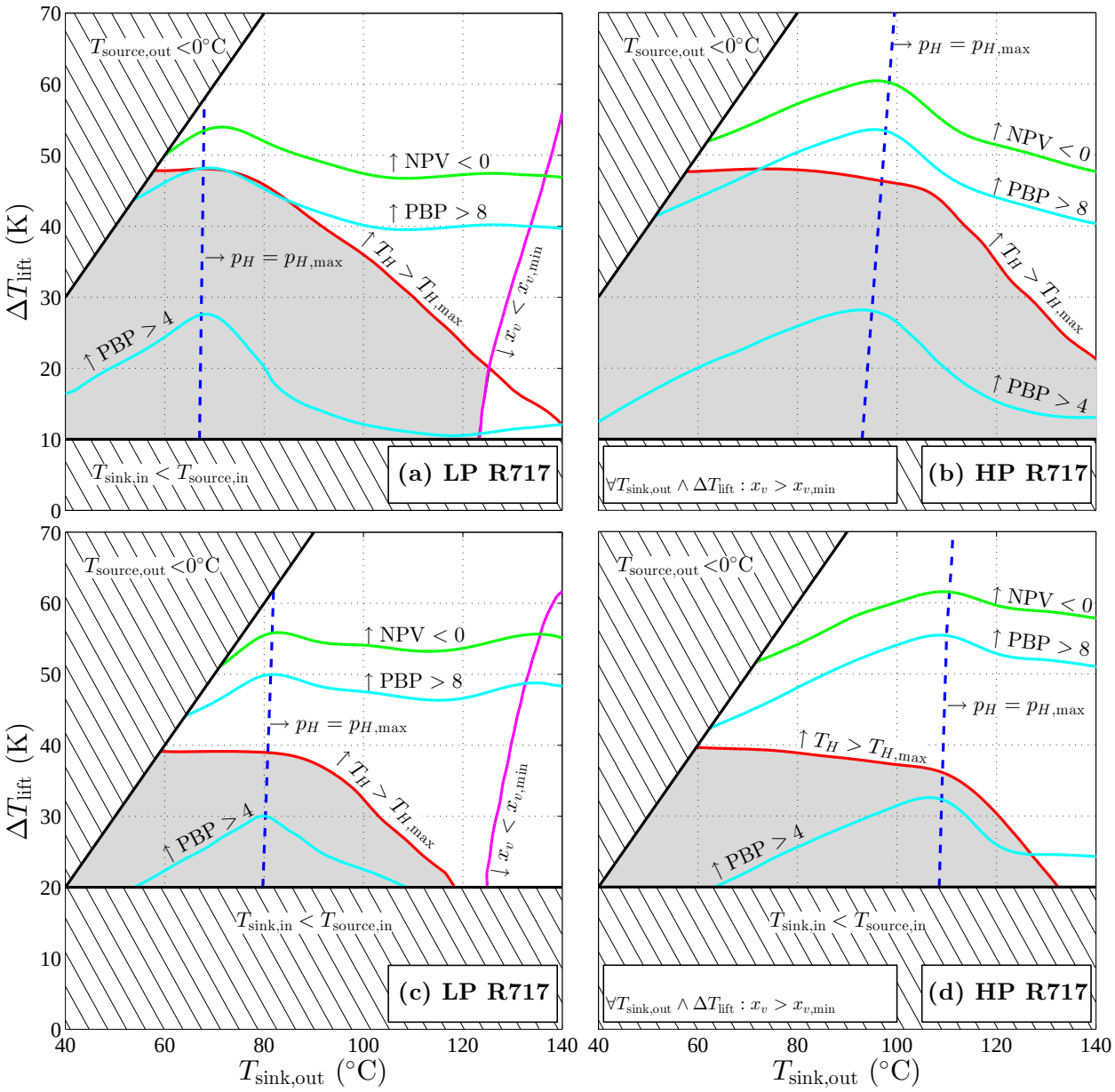

Figure 5: Feasible working domains indicated by grey background for HACHP using LP R717 and HP R717 compressors at ΔT_{sink}=10 K, ΔT_{source}=10 K (a) and (b) and ΔT_{sink}=20 K, ΔT_{source}=20 K (c) and (d). Hatched areas define technically infeasible domains. Curves indicate technical operating limits of components and economic limits

ble heat supply temperatures compared to those concluded from Brunin et al. (1997). This is mainly due to the applied constraint on the compressor discharge temperature, which was neglected in Brunin et al. (1997). The use of a cooled screw compressor or an oil free compressor could relax the constraints on the compressor discharge temperature and allow heat supply temperatures above 150 °C. Alternatively, the application of a gas cooler prior to the mixing of vapour and lean solution can reduce the compressor discharge temperature as shown in Jensen et al. (2014). Further, a two-stage compression could be a measure of reducing the compressor discharge temperature and thus extending the working domain of the HACHP.

5. Conclusion

The feasible working domain of a HACHP has been evaluated based on a detailed economic analysis and a comprehensive investigation of the design variables: ammonia mass fraction and circulation ratio. The results show that the HACHP is capable of delivering both higher heat supply temperatures and higher temperature lifts than conventional VCHP.

Heat supply temperatures up to 150 °C and temperature lifts up to 60 K can be attained with commercially available components and with an economic benefit compared to gas combustion. It is found that the dominating constraint for the HACHP is the compressor discharge temperature. Further, it is found

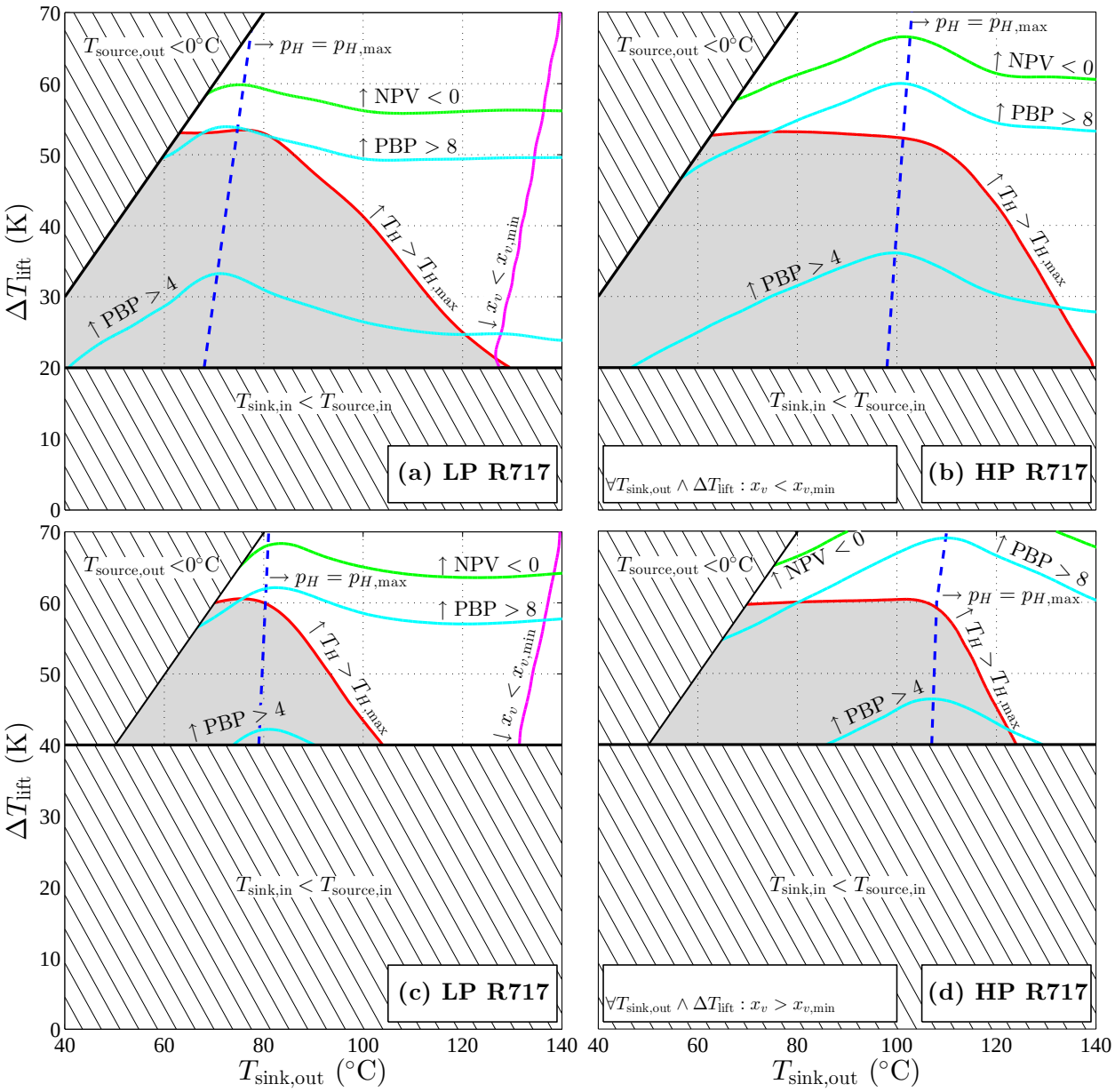

Figure 6: Working domains for HACHP using LP R717 and HP R717 compressors at at ΔT_{sink}=20 K, ΔT_{source}=10 K (a) and (b) and ΔT_{sink}=40 K, ΔT_{source}=10 K (c) and (d)

that reducing the sink/source temperature difference increases the maximum attainable heat supply temperature while reducing the maximum attainable lift.

When comparing the PV of the HACHP with the VCHP at the operating points where both are applicable: the cost of the HACHP is lower for almost all operating conditions with a heat supply temperature above 80 °C. For the range where the HACHP competes with R717 the difference in PV can be insignificant and both technologies should be considered. For the high temperature range where the only applicable VCHP technology is R600a the difference in PV is large and the HACHP should be applied.

Acknowledgements

This research project is financially funded by EUDP (Energy Technology Development and Demonstration), project title: "Development of ultra-high temperature hybrid heat pump for process application", project number: 64011-0351 and by the Copenhagen Cleantech Cluster (CCC), DONG Energy and the Danish Technological Institute.

References

Abu-Khader, M.M., 2012, Plate heat exchangers: Recent advances. Renew. sust. energ. rev., 16(4):1883 – 1891. ISSN 1364-0321. doi: http://dx.doi.org/10.1016/j.rser.2012.01.009.

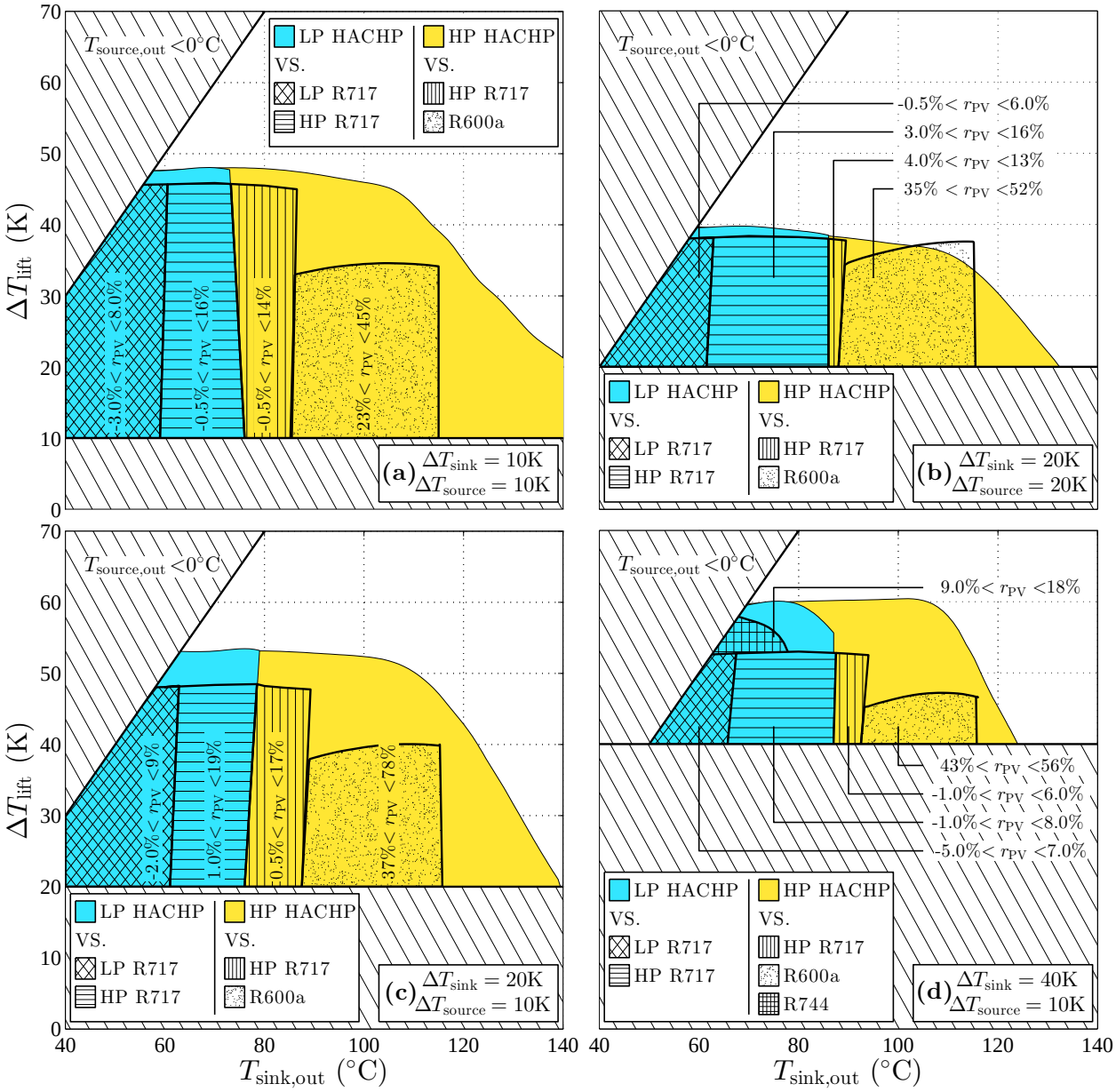

Figure 7: Most profitable HACHP and comparison with the best available VCHP. The blue area indicates the region in which the NPV of the LP R717 is higher than the NPV of the HP R717 solution. The hatched areas indicate which VCHP is the best competing technology.

Ahlsell Danmark ApS., 2013, Priskatalog 2013. [accessed 26.09.13]. URL https://webshop.ahlsell.com/vivp/index.jsp

Altenkirch, E., 1950, Kompressionskältemachine mit lösungskreislauf. Kältetechnik, 2(10,11,12):251–259,310–315,279–284.

Annex–21, 1995, Industrial Heat Pumps - Experiences, potential and Global Environmental Benefits. IEA Heat Pump Centre.

Bejan, A., Tsatsaronis, G., Moran, M.J., 1996, Thermal Design and Optimization. Wiley-Interscience publication. Wiley. ISBN 9780471584674.

Bell, K.J., Ghaly, M.A., 1972, An approximate generalized design method for multicomponent/partial condensers. In 13th National Heat Transfer Conference, Denver, Colorado, USA. AIChE-ASME.

Berntsson, T., Hultén, M., 1999, The compression/absorption cycle – influence of some major parameters on COP and a comparison with the compression cycle compression – absorption. Int. J. Refrigeration, 22:91–106.

Berntsson, T. Hultén, M., 2002, The compression / absorption heat pump cycle - conceptual design improvements and comparisons with the compression cycle. Int. J. Refrigeration, 25:487–497.

Brunin, O., Feidt, M., Hivet, B., 1997, Comparison of the working domains of some compression heat pumps and a compression-absorption heat pump. Int. J. Refrigeration, 20(5):308 – 318. ISSN 0140-7007.

Conde, M., 2004, Thermophysical properties of NH3 + H2O solutions for the industrial design of absorption refrigeration equiptment. Technical report, M. Conde Engineering.

Corberan, J.M., 2011, 2nd IIR workshop on refrigerant charge reduction in refrigerating systems. Int. J. Refrigeration, 34(2):600, 3.

Danish Energy Agency., 2013, Data, tables, statistics and maps, energy in denmark 2012. [accessed 30.06.14].

El-Sayed, Y.M., On exergy and surface requirements for heat transfer processes involving binary mixtures. In: Proceedings of ASME Winter Annual Meeting, Chicago, 1988. ASME-AES Vol. 6, HTD - Vol. 97, 19–24.

F-Chart, S.L., 1992, Engineering Equation Solver (EES). http://www.fchart.com/ees. [accessed 30.06.14].

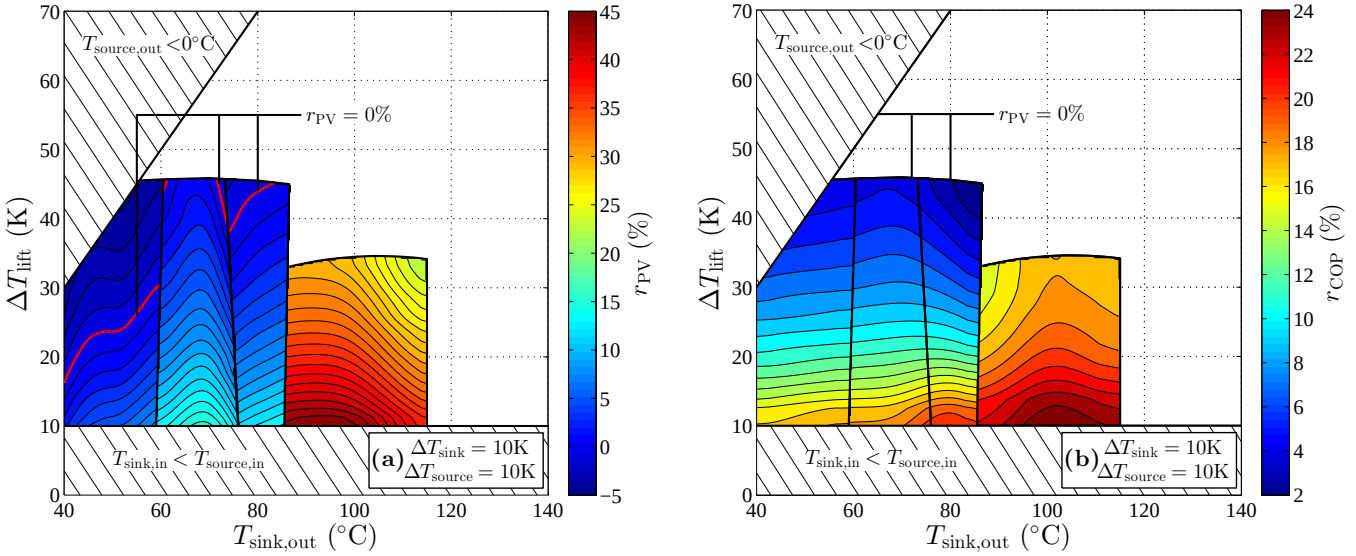

Figure 8: Contours of relative difference in PV, r_{PV}, (a) and the relative difference in COP, r_{COP}, between the best available HACHP and VCHP. Both for a sink/source configuration of 10K/10K

FK Teknik A/S., 2013, Priskatalog 2013. [accessed 26.09.13]. URL http://www.fkteknik.dk/kataloger.html

Grundfos DK A/S., 2014, Indicative retail prices.

H. Jessen Jürgensen A/S., 2013, Price catalog 2013. [accessed 26.09.13]. http://www.hjj.dk/indhold_prisliste.html .

Hybrid Energy AS., 2015, [accessed 28.01.15]. URL http://www.hybridenergy.no/en/clients/

Ibrahim, O.M. Klein, S.A., 1993, Thermodynamic Properties of Ammonia-Water Mixtures. In ASHRAE Trans.: Symposia, pages 21, 2 1495–1502.

Itard, L.C.M. Machielsen, C.H.M., 1994, Considerations when modelling compression/resorption heat pumps. Int. J. Refrigeration, 17(7):453–460.

Jensen, J.K., Reinholdt, L., Markussen, W.B., Elmegaard, B., 2014, Investigation of ammonia/water hybrid absorption/compression heat pumps for heat supply temperatures above 100°C. In International Sorption Heat Pump Conference, March 31 - April 2, University of Maryland, Washington D.C.

Johnson Controls., 2013, HPO R717 compressor cost. personal communication with Sørensen, K.

Kemp, I.C., 2011, Pinch Analysis and Process Integration: A User Guide on Process Integration for the Efficient Use of Energy Elsevier Science ISBN: 9780080468266.

Lorenz, H., 1894, Beiträge zur Beurteilung von Kühlmaschinen. Z VDI, 38: 62–68, 98–103, 124–130.

Martin, H., 1996, A theoretical approach to predict the performance of chevron-type plate heat exchangers. Chemical Engineering and Processing: Process Intensification, 35(4):301 – 310. ISSN 0255-2701.

Ommen, T., Markussen, C.M., Reinholdt, L., Elmegaard, B., 2011, Thermoeconomic comparison of industrial heat pumps. In ICR 2011, August 21 - 26 - Prague, Czech Republic.

Ommen, T., Jensen, J.K., Markussen, W.B., Reinholdt, L., Elmegaard, B., 2014 Technical and economic working domains of industrial heat pumps 1: vapour compression heat pumps. Int. J. Refrigeration. note:[Submitted].

Ommen, T., Markussen, W.B., Elmegaard, B., 2014 Heat pumps in combined heat and power systems. Energy, 79: 989–1000, Nov. doi:10.1016/j.energy.2014.09.016.

Osenbrück, A., 1895, Verfahren zur Kälteerzeugung bei Absorptionsmaschinen. Deutsches Reichspatent, [DRP 84084].

Radermacher, R. Hwang, Y., 2005, Vapor Compression Heat Pumps with Refrigerant Mixtures. Mechanical Engineering. Taylor & Francis. ISBN 9781420037579.

Silver, L., 1947, Gas cooling with aqueous condensation: A new procedure for calculating heat transfer coefficients. The Industial Chemist, pages 380–386, June.

Stoecker, W., 1998, Industrial Refrigeration Handbook. McGraw-Hill Education. ISBN 9780070616233.

SWEP international AB., 2014, Technical information v120t anf v10t. [accessed 01.06.14]. URL http://www.swep.net/en.

SWEP International AB., 2014, private communication SWEP - products & solutions (B400, B120T F-pressure, B17 product sheets) - non-disclosure agreement URL http://www.swep.net/en/products_-solutions/productfinder/Pages/B120T.aspx.

Táboas, F., Vallès, M., Bourouis, M., Coronas, A., 2012, Assessment of boiling heat transfer and pressure drop correlations of ammonia/water mixture in a plate heat exchanger. Int. J. Refrigeration, 35(3):633–644, May. ISSN 01407007.

Townsend, D., Linnhoff, B., 1983, Heat and power networks in process design. Part I: Criteria for placement of heat engines and heat pumps in process networks. AIChE Journal, 35(3):742–748, 29.

Yan, Y.Y, Lio, H.C., Lin, T.F., 1999, Condensation heat transfer and pressure drop of refrigerant r-134a in a plate heat exchanger. Int. J. Heat Mass Tran., 42(6):993–1006.

Zheng, N., Song, W., Zhao, L., 2013, Theoretical and experimental investigations on the changing regularity of the extreme point of the temperature difference between zeotropic mixtures and heat transfer fluid. Energy, 55: 541–552, June . ISSN 03605442.

Appendix A. Heat transfer and pressure drop correlations

Table A.1: Heat transfer and pressure drop correlations

General equations

$$G = \frac{\dot{m}}{M \cdot W \cdot b} \quad \text{(A.1)}$$

$$\mathrm{Re} = \frac{G \cdot D_h}{\mu} \quad \text{(A.2)}$$

$$\mathrm{Re_{lo}} = \frac{G \cdot D_h}{\mu_{\mathrm{lo}}} \quad \text{(A.3)}$$

$$\mathrm{Bo} = \frac{\dot{Q}}{G \cdot h_{\mathrm{fg}} \cdot A_{\mathrm{HT}}} \quad \text{(A.4)}$$

Martin (1996)

$$\varphi = \beta - 90° \quad \text{(A.5)}$$

$$\phi = \frac{1}{6}\left(1 + \sqrt{1 + \frac{b\pi}{\Lambda^2}} + 4\sqrt{1 + \frac{b\pi}{2\Lambda^2}}\right) \quad \text{(A.6)}$$

If $\frac{\mathrm{Re}}{\phi} < 2000$:

$$\xi_0 = \frac{64\phi}{\mathrm{Re}} \quad \text{(A.7)}$$

$$\xi_{1.0} = \frac{597\phi}{\mathrm{Re}} + 3.85 \quad \text{(A.8)}$$

If $\frac{\mathrm{Re}}{\phi} \geq 2000$:

$$\xi_0 = \left(1.8 \log_{10} \frac{\mathrm{Re}}{\phi} - 1.5\right)^{-2} \quad \text{(A.9)}$$

$$\xi_{1.0} = \frac{39}{(\mathrm{Re}/\phi)^{0.289}} \quad \text{(A.10)}$$

$$\frac{1}{\xi} = \frac{\cos\varphi}{\sqrt{0.18\tan\varphi + 0.36\sin\varphi + \xi_0/\cos\varphi}} + \frac{1 - \cos\varphi}{\sqrt{3.8\xi_{1.0}}} \quad \text{(A.11)}$$

$$\mathrm{Nu} = \phi \cdot 0.122 \cdot \mathrm{Pr}^{1/3} \frac{\mu}{\mu_w}^{1/6} \left(\xi \cdot \left(\frac{\mathrm{Re}}{\phi}\right)^2 \sin(2\varphi)\right)^{0.374} \quad \text{(A.12)}$$

$$\alpha = \frac{\mathrm{Nu} \cdot \lambda}{D_h} \quad \text{(A.13)}$$

$$\Delta p = \frac{2 \cdot \xi \cdot G^2 \cdot v \cdot L_{\mathrm{HT}}}{D_h} \quad \text{(A.14)}$$

Yan et al. (1999)

$$G_{\mathrm{eq}} = G\left(1 - q + q\left(\frac{v_{\mathrm{vo}}}{v_{\mathrm{lo}}}\right)^{1/2}\right) \quad \text{(A.15)}$$

$$\mathrm{Re_{eq}} = \frac{G_{\mathrm{eq}} \cdot D_h}{\mu_{\mathrm{lo}}} \quad \text{(A.16)}$$

$$\alpha = \frac{\lambda}{D_h} \cdot 4.188 \cdot \mathrm{Re_{eq}}^{0.4} \cdot \mathrm{Pr_{lo}}^{1/3} \quad \text{(A.17)}$$

$$\xi \cdot \mathrm{Re_{lo}}^{0.4} \cdot \mathrm{Bo}^{-0.5} \cdot \left(\frac{p}{p_c}\right)^{-0.8} = 94.75 \cdot \mathrm{Re_{eq}}^{-0.0467} \quad \text{(A.18)}$$

Bell and Ghaly (1972)

$$\alpha = \left(\frac{1}{\alpha_{\mathrm{lf}}} + \frac{Z}{\alpha_{\mathrm{vo}}}\right)^{-1} \quad \text{(A.19)}$$

$$Z = q \cdot c_{p,\mathrm{v}} \cdot \frac{dT}{dh} \quad \text{(A.20)}$$

Táboas et al. (2012)

$$X_{\mathrm{tt}} = \left(\frac{\mu_{\mathrm{lo}}}{\mu_{\mathrm{vo}}}\right)^{0.1} \left(\frac{1-q}{q}\right)^{0.9} \left(\frac{v_{\mathrm{lo}}}{v_{\mathrm{vo}}}\right)^{0.5} \quad \text{(A.21)}$$

$$F = \left(1 + \frac{3}{X_{\mathrm{tt}}} + \frac{1}{X_{\mathrm{tt}}^2}\right)^{0.2} \quad \text{(A.22)}$$

$$u_{\mathrm{SL}} = G \cdot (1 - q) \cdot v_{\mathrm{lo}} \quad \text{(A.23)}$$

$$u_{\mathrm{SV}} = G \cdot q \cdot v_{\mathrm{vo}} \quad \text{(A.24)}$$

If: $u_{\mathrm{SV}} < 111.88 \cdot u_{\mathrm{SL}} + 11.848 \quad \mathrm{ms}^{-1}$:

$$\alpha = 5 \cdot \mathrm{Bo}^{0.15} \alpha_{\mathrm{lo}} \quad \text{(A.25)}$$

If: $u_{\mathrm{SV}} > 111.88 \cdot u_{\mathrm{SL}} + 11.848 \quad \mathrm{ms}^{-1}$:

$$\alpha = F \cdot \alpha_{\mathrm{lo}} \quad \text{(A.26)}$$

$$\xi_{\mathrm{lo}} = 4.779 \cdot \mathrm{Re_{lo}}^{-0.118} \quad \text{(A.27)}$$

$$\Delta p = \frac{2 \cdot \xi_{\mathrm{lo}} \cdot F \cdot G^2 \cdot v_{\mathrm{lo}} \cdot L_{\mathrm{HT}}}{D_h} \quad \text{(A.28)}$$

Appendix B. Detailed results of the thermodynamic, heat transfer and economic models

Table B.1: Thermodynamic state points for a HACHP with x_r = 0.65 and f = 0.65, $T_{\text{sink,out=}}$ = 80 °C, ΔT_{lift} = 30 K and ΔT_{sink} = ΔT_{source} = 20 K

j^{th} stream	media	$\dot{m}_j$ (kg s^{-1})	x_j (-)	T_j (°C)	p_j (bar)	h_j (kJ kg^{-1})	s_j (kJ kg^{-1} K^{-1})	v (10^{-3} m^3 kg^{-1})
(1)	NH_3-H_2O	1.929	0.650	45.00	4.957	459.1	2.07	106
(2)	NH_3-H_2O	0.6750	0.993	45.00	4.957	1382	4.95	300
(3)	NH_3-H_2O	0.6750	0.993	169.9	17.60	1653	5.08	118
(4)	NH_3-H_2O	1.929	0.650	91.01	17.60	609.2	2.31	31.8
(5)	NH_3-H_2O	1.929	0.650	65.62	17.59	90.98	0.832	1.39
(6)	NH_3-H_2O	1.929	0.650	54.25	17.39	37.01	0.670	1.36
(7)	NH_3-H_2O	1.929	0.650	24.85	4.964	37.01	0.697	30.0
(8)	NH_3-H_2O	1.254	0.465	44.91	4.957	-37.86	0.512	1.21
(9)	NH_3-H_2O	1.254	0.465	45.12	17.51	-35.96	0.513	1.21
(10)	NH_3-H_2O	1.254	0.465	63.58	17.60	47.07	0.766	1.24
(11)	Water	11.94		60.00	2.000	251.3	0.831	
(12)	Water	11.94		80.00	1.875	335.0	1.08	
(13)	Water	9.738		50.00	2.000	209.5	0.704	
(14)	Water	9.738		30.00	1.929	125.8	0.436	

Table B.2: Heat and work load COP and volume flow rates and receiver model

$\dot{W}_{\text{Comp.}}$	183.1	kW	$\dot{Q}_{\text{Absorber}}$	1000	kW	COP	5.122	-
$\dot{W}_{\text{Comp.,el}}$	192.7	kW	$\dot{Q}_{\text{Desorber}}$	814.5	kW	$\dot{V}_2$	0.2024	m^3 s^{-1}
$\dot{W}_{\text{Pump}}$	2.39	kW	$\dot{Q}_{\text{IHEX}}$	104.1	kW	$\dot{V}_{\text{dis}}$	0.2530	m^3 s^{-1}
$\dot{W}_{\text{Pump,el}}$	2.514	kW				V_4	0.1106	m^3

Table B.3: HEX dimensions, heat transfer and pressure drop coefficients and refrigerant charge estimation

Absorber:			Desorber:			Internal HEX:		
Plate type	SWEP V120T		Plate type	SWEP V120T		Plate type	SWEP V120T	
$\bar{\alpha}_{\text{tp}}$	7.30	kWm^{-2}K^{-1}	$\bar{\alpha}_{\text{tp}}$	5.847	kW m^{-2} K^{-1}	$\bar{\alpha}_r$	10.36	kW m^{-2} K^{-1}
$\bar{\alpha}_{\text{sink}}$	8.484	kWm^{-2}K^{-1}	$\bar{\alpha}_{\text{source}}$	5.58	kW m^{-2} K^{-1}	$\bar{\alpha}_l$	6.587	kW m^{-2} K^{-1}
$\bar{\xi}_{\text{tp}}$	0.03352	-	$\bar{\xi}_{\text{tp}}$	5.036	- ($\xi_{\text{lo}} \cdot F$)	$\bar{\xi}_r$	1.941	-
$\bar{\xi}_{\text{sink}}$	2.037	-	$\bar{\xi}_{\text{source}}$	2.241	-	$\bar{\xi}_l$	2.174	-
Δp_{3-4}	0.0008421	bar	Δp_{7-1}	0.007692	bar	Δp_{5-6}	0.204	bar
Δp_{11-12}	0.1255	bar	Δp_{14-13}	0.07065	bar	Δp_{9-10}	0.08604	bar
U	3.495	kWm^{-2}K^{-1}	U	2.621	kW m^{-2} K^{-1}	U	3.577	kW m^{-2} K^{-1}
$\Delta \bar{T}_{\text{LM}}$	6.551	K	$\Delta \bar{T}_{\text{LM}}$	6.286	K	ΔT_{LM}	4.725	K
N	353	-	N	400	-	N	52	-
A_{HT}	43.67	m^2	A	49.43	m^2	A_{HT}	6.163	m^2
A_{IN}	45.03	m^2	A_{IN}	51.03	m^2	A_{IN}	6.634	m^2
m	25.08	kg	m	28.59	kg	m	8.997	kg

Table B.4: PEC, TCI, total HACHP investment and operational cost

Break down of HACHP TCI costs						Break down of HACHP FC, OMC, NPV and PBP		
k^{th}	component	X_Y		PEC$_Y$ (€)	TCI$_k$ (€)		PV (€)	Annual Costs (€)
(1)	Compressor	910.8	m^3 h^{-1}	34944	145365	TCI$_{\text{HP}}$	415864.8	-
	Compressor motor	183.1	kW	8747.7	36390.4	TCI$_{\text{NG}}$	0	-
(2)	Pump	2.514	kW	2243.7	9333.94	FC$_{\text{HP}}$	590247.6	56489.6
(3)	Absorber	45.03	m^2	16356	68038.9	FC$_{\text{NG}}$	1435741	137407
(4)	Receiver	0.1116	m^3	1656.6	6891.57	OMC$_{\text{HP}}$	83172.76	7960.04
(5)	Internal HEX	6.163	m^2	3533.8	14700.8	OMC$_{\text{NG}}$	0	0
(6)	Desorber	51.03	m^2	18076	75194.4	PV$_{\text{HP}}$	1089284	-
(7)	LVS	728.7	m^3 h^{-1}	14411	59948.7	PV$_{\text{NG}}$	1435741	-
						Annual net cash flow		72957.4
Total HACHP investment					415864	NPV	346456.5	-
						PBP	-	5.70